

BIMODALITY OF CIRCUMSTELLAR DISK EVOLUTION INDUCED BY HALL CURRENT

Y. TSUKAMOTO^{1,2}, K. IWASAKI^{2,3}, S. OKUZUMI⁴, M. N. MACHIDA⁵, AND S. INUTSUKA²

Draft version March 5, 2022

ABSTRACT

The formation process of circumstellar disks is still controversial because of the interplay of complex physical processes that occurs during the gravitational collapse of prestellar cores. In this study, we investigate the effect of the Hall current term on the formation of the circumstellar disk using three-dimensional simulations. In our simulations, all non-ideal effects as well as the radiation transfer are considered. The size of the disk is significantly affected by a simple difference in the inherent properties of the prestellar core, namely whether the rotation vector and the magnetic field are parallel or anti-parallel. In the former case, only a very small disk (< 1 AU) is formed. On the other hand, in the latter case, a massive and large (> 20 AU) disk is formed in the early phase of protostar formation. Since the parallel and anti-parallel properties do not readily change, we expect that the parallel and anti-parallel properties are also important in the subsequent disk evolution and the difference between the two cases is maintained or enhanced. This result suggests that the disk size distribution of the Class 0 young stellar objects is bimodal. Thus, the disk evolution can be categorized into two cases and we may call the parallel and anti-parallel systems as *Ortho-disk* and *Para-disk*, respectively. We also show that the anti-rotating envelopes against the disk-rotation appear with a size of $\gtrsim 200$ AU. We predict that the anti-rotating envelope will be found in the future observations.

1. INTRODUCTION

Circumstellar disks are born around protostars in the course of the self-gravitational collapse of the molecular cloud cores. The angular momentum evolution during the collapse is critical for the disk formation because the disks are supported by centrifugal force.

The magnetic field plays a central role for the angular momentum evolution. During the gravitational collapse, a toroidal magnetic field is created by the rotation, and the magnetic tension decelerates the gas rotation, removing the angular momentum. This effect is known as magnetic braking (Mouschovias and Paleologou 1979). Previous studies using ideal magnetohydrodynamics (MHD) simulations have shown that, for a typical magnetic field strength, the disk formation is completely suppressed in the early Class 0 phase (Mellon and Li 2008; Hennebelle and Fromang 2008; Bate *et al.* 2014).

Meanwhile, the observations of Class 0 young stellar objects (YSOs) showed that a relatively large circumstellar disk ($r \sim 50$ AU) exists around young protostars (Ohashi *et al.* 2014; Sakai *et al.* 2014; Tobin *et al.* 2015). These observations indicate that some very young protostars have relatively large circumstellar disks with a size of $r > 10$ AU, suggesting a disagreement between the previous theoretical works and the observations.

Possible physical mechanisms for resolving the discrepancy between theory and observation are the Ohmic and ambipolar diffusion (Mellon and Li 2009; Machida *et al.* 2014; Tomida *et al.* 2015; Tsukamoto *et al.* 2015a). Pre-

vious works following the formation of protostars showed that a small disk with size of $r \lesssim 1$ AU is formed around the protostar when the magnetic diffusion are considered (Tomida *et al.* 2013; Tsukamoto *et al.* 2015a). However, the formation of a disk with a size of $r \gtrsim 10$ AU at the early phase of protostar formation in a typically magnetized cloud core is still highly difficult even with these effects.

The effect of the Hall current term is the least studied effect in the context of disk formation. The Hall current term generates a toroidal magnetic field from a poloidal magnetic field and directly affects the magnetic tension that determines the magnetic braking efficiency. The Hall current term in MHD equations is not invariant against the global inversion of the magnetic field (Wardle and Ng 1999; Krasnopolsky *et al.* 2011; Li *et al.* 2011; Braiding and Wardle 2012) and its effect changes depending on whether rotation vector and magnetic field of host cloud core are parallel or anti-parallel. When the Hall diffusion coefficient is negative (this is true for $\rho \lesssim 10^{-11}$ g cm⁻³ in our model, see figure 4) and the rotation vector and the magnetic field are anti-parallel, the Hall current term weakens the magnetic braking. Meanwhile, the Hall current term strengthens the magnetic braking in the parallel case. Despite the possible importance of the Hall current term in the disk evolution, it is still unclear how the Hall current term affects the formation of the circumstellar disk because the previous numerical studies (Krasnopolsky *et al.* 2011; Li *et al.* 2011) neglected the first core evolution phase, which plays an important role in the disk formation (Machida and Matsumoto 2011; Dapp *et al.* 2012; Tomida *et al.* 2015; Tsukamoto *et al.* 2015a) and simplified the radiative transfer. Three-dimensional simulations are also necessary for investigating non-axisymmetric effects.

In this paper, we performed three-dimensional simulations starting from prestellar cloud cores. Our numerical

¹ Laboratory of Computational Astrophysics, RIKEN, Saitama, Japan

² Department of Physics, Nagoya University, Aichi, Japan

³ Department of Environmental Systems Science, Faculty of Science and Engineering, Doshisha University, Kyoto, Japan

⁴ Department of Earth and Planetary Sciences, Tokyo Institute of Technology, Tokyo, Japan

⁵ Department of Earth and Planetary Sciences, Kyushu University, Fukuoka, Japan

simulations include all non-ideal MHD effects as well as the radiative transfer. The simulations were conducted until the birth of the protostar. We did not use any sink technique for the center and hence our simulations do not suffer from numerical artifacts introduced by sink particle or the inner boundary which may artificially change the formation and evolution of the disk (Machida *et al.* 2014).

2. NUMERICAL METHOD AND INITIAL CONDITIONS

In this study, we solved the non-ideal radiation magneto-hydrodynamics equations with self-gravity. The numerical method, except for the Hall current term, is the same as that used in our previous study (Tsukamoto *et al.* 2015a). The ideal MHD part was solved using the methods proposed by Iwasaki and Inutsuka (2011, 2013). The radiative transfer was treated with the methods of (Whitehouse and Bate 2004; Whitehouse *et al.* 2005). We treated the Ohmic and ambipolar diffusion with the method described by Tsukamoto *et al.* (2013a) and Wurster *et al.* (2014), respectively. Both diffusion processes were accelerated by super time stepping (Alexiades *et al.* 1996).

For this study, we newly implemented the Hall current term according to Wurster *et al.* (2014). The Hall current term couples with the ideal terms and changes the phase velocity. Thus, it is unclear that the sub-cycle method, which is often used for the diffusion terms (Machida *et al.* 2011a; Tsukamoto *et al.* 2015a), is valid for the Hall current term. Therefore, in our simulations, the ideal MHD term and the Hall current term are updated with the same time-step. The smaller time-step of either the ideal term or the Hall current term, $\Delta t_{\text{Hall}} = C_{\text{hall}} h^2 / (4\pi |\eta_{\text{H}}|)$ (Sano and Stone 2002) is used for the update. Here, $C_{\text{hall}} = 0.4$ is the Courant-Friedrichs-Levy number for the Hall term, and h is the smoothing length.

We conducted the numerical tests for the Hall current term and confirmed that the scheme can correctly calculate the whistler mode in the linear wave propagation test. Furthermore, we conducted gravitational collapse tests of non-rotating cloud cores and confirmed that the rotation amplitude induced by the Hall current term does not depend on the direction of the magnetic field. We adopted the equation of state (EOS), and dust and gas opacity tables from Tomida *et al.* (2013), Semenov *et al.* (2003), and Ferguson *et al.* (2005), respectively. We employed the resistivity table used in our previous works (Okuzumi 2009; Tsukamoto *et al.* 2015a) in which the fixed dust grain size of $a = 0.035 \mu\text{m}$ and fixed cosmic-ray ionization rate of $\xi_{\text{CR}} = 10^{-17} \text{s}^{-1}$ are assumed.

We modeled the initial cloud core with an isothermal uniform gas sphere using about 3×10^6 particles. The mass and temperature of the initial core are $1 M_{\odot}$ and 10 K, respectively. Initially, the core has a radius of $R = 3.0 \times 10^3$ AU and is rigidly rotating with an angular velocity of $\Omega_0 = 2.2 \times 10^{-13} \text{s}^{-1}$. The initial magnetic field is uniform and parallel to the rotation (z -) axis with a magnitude of $B_0 = 1.7 \times 10^2 \mu\text{G}$. The corresponding initial mass-to-flux ratio relative to the critical value is $\mu = (M/\Phi)/(M/\Phi)_{\text{crit}} = 4$ where $\Phi = \pi R^2 B_0$ and $(M/\Phi)_{\text{crit}} = (0.53/3\pi)(5/G)^{1/2}$ (Mouschovias and Spitzer 1976).

We conducted three simulations, Model Para, Ortho, and NoHall. The magnetic field and the rotation vector are initially perfectly parallel in Model Ortho, NoHall and anti-parallel in Model Para. The model NoHall does not include the Hall current term. Other parameters are the same in the models. The runtime of Models Para, Ortho, and NoHall was about 3.7×10^5 , 1.4×10^5 , 1.6×10^4 CPU hours, respectively with XC30 in NAOJ.

A boundary condition is imposed at $R_{\text{out}} = 0.995R$, and the particles with $r > R_{\text{out}}$ rotate with an initial angular velocity. Thus, the gas is confined in a rigidly rotating shell. This boundary is very similar to that used in Matsumoto and Tomisaka (2004); Machida *et al.* (2007) and also used in our previous work (Tsukamoto *et al.* 2015a). In addition, a boundary condition for radiative transfer is introduced by fixing the gas temperature to be 10 K when $\rho < 2.0 \times 10^{-17} \text{g cm}^{-3}$.

3. RESULTS

In figure 1, we show the structure at the center of the cloud core. The left and right panels show the result of Models Para and Ortho, respectively. The central densities are 10^{-9}g cm^{-3} for the left panels, which correspond to slightly before the protostar formation, and 10^{-2}g cm^{-3} for the right panels, which is immediately after the protostar formation.

When the rotation vector and magnetic field are in the anti-parallel configuration, a large disk with a size of $r \sim 20$ AU is formed (Model Para; top left panel). The disk is so massive that spiral arms are created by the gravitational instability. We confirmed that the Toomre's Q value, $Q = \kappa_{\text{ep}} c_s / (\pi G \Sigma)$ is $Q \sim 1$ in the entire disk region ($5 \lesssim r \lesssim 20$ AU). In the top panel of figure 2, we show the force balance between the pressure gradient force, the centrifugal force, and the radial gravitational force on the x -axis. The gas is mainly supported by the centrifugal force. Therefore, a rotationally-supported massive disk is formed in Model Para. On the other hand, when the rotation vector and magnetic field are in the parallel configuration, no large disk ($r \gtrsim 10$ AU) appears (Model Ortho; top right panel) because the magnetic braking is strengthened by the Hall current term and the angular momentum is efficiently removed from the central region. The dense region ($\rho > 10^{-11} \text{g cm}^{-3}$) at the center, which has a radius of $r \sim 5$ AU, is the remnant of the first core and is not a rotationally-supported disk. Although a rotationally-supported disk with $r \lesssim 0.6$ AU is also formed in Model Ortho around the protostar, as shown in the bottom panel of the figure 2; the difference of the disk size of Model Para and Model Ortho is remarkable.

The plasma β in the disk regions ($r \lesssim 20$ AU) of Model Para is large ($\beta > 100$) because the magnetic flux is largely removed due to the magnetic diffusion. In this high β region, the magnetic field and the gas are almost decoupled and the magnetic braking is no longer important. The disk is sufficiently massive and develops gravitational instability. Thus, gravitational instability may play an important role for angular momentum transfer in the subsequent evolutionary phase. Furthermore, in such a massive extended disk, disk fragmentation, which is a promising mechanism for the formation of binaries or wide-orbit planets, (Marois *et al.* 2010) possibly occurs in the subsequent evolution (Boss 1997; Inutsuka *et al.*

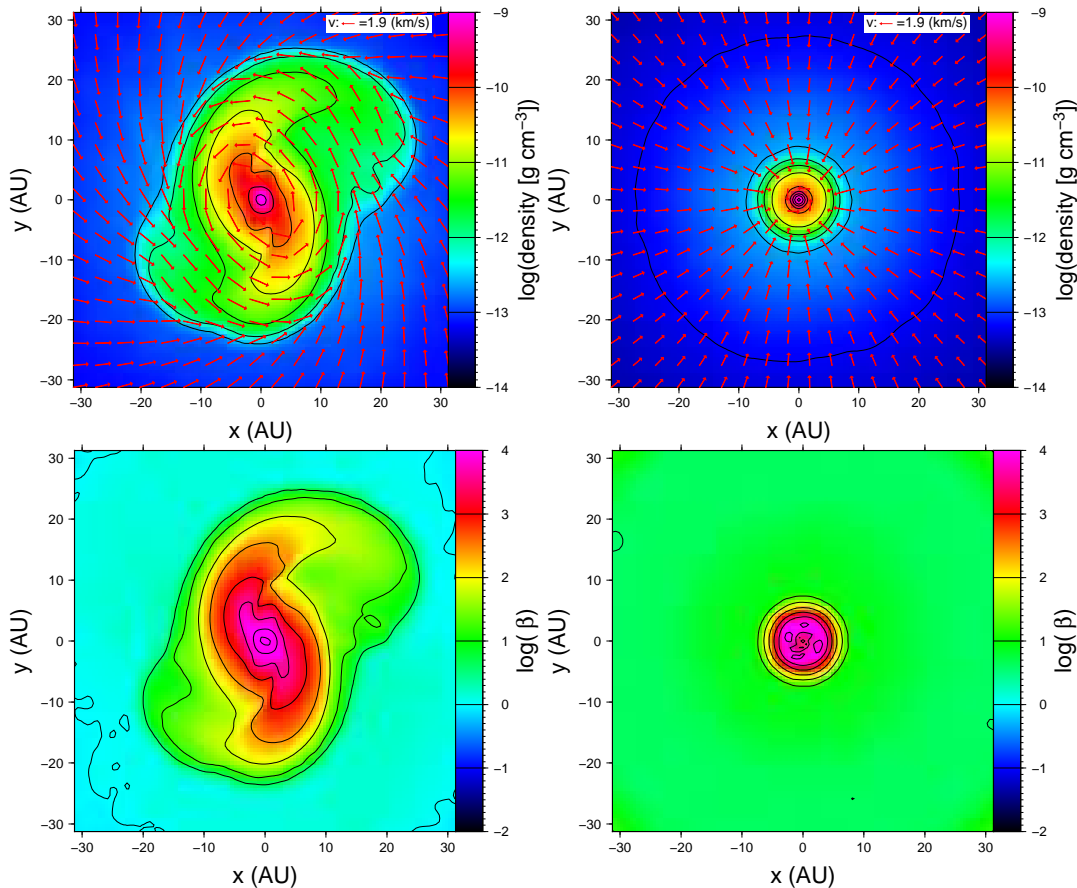


FIG. 1.— Cross sections of the density (top panels) and the plasma β (bottom panels) in the x - y plane. The left panels show the results of Model Para, while the right panels show those of Model Ortho. The central densities at these snapshots are 10^{-9} g cm^{-3} and 10^{-2} g cm^{-3} for the left and right panels, respectively.

2010; Machida *et al.* 2011b; Tsukamoto and Machida 2011, 2013; Tsukamoto *et al.* 2013b, 2015b). Thus, the parallel or anti-parallel property of the cloud core would play a crucial role for the formation of the binary or wide-orbit planets.

To quantify the strength of the rotation at the center of the cloud core, we show the mean specific angular momentum of regions with $\rho > 10^{-12}$ g cm^{-3} as a function of the central density in figure 3. The figure shows that the specific angular momentum in Model Para is about an order of magnitude larger than that of Model Ortho. The specific angular momentum in Model Ortho (Para) is about three times smaller (larger) than that in Model NoHall. The combination of the spin-up effect (weakening of the magnetic braking) in the anti-parallel case and the spin-down effect (strengthening of the magnetic braking) in the parallel case causes the large difference.

The mass and the magnetic flux $\Phi = \int \mathbf{B} d\mathbf{S}$ of regions with $\rho > 10^{-12}$ g cm^{-3} in model Para, Ortho, and NoHall at the beginning of the second collapse ($\rho_c = 10^{-8}$ g cm^{-3}), was (M (M_\odot), Φ (G cm^2)) = (1.9×10^{-1} , 3.7×10^{28}), (7.5×10^{-2} , 4.1×10^{27}), and (1.1×10^{-1} , 8.0×10^{27}), respectively. Here, $d\mathbf{S}$ is defined at the $z = 0$ and is parallel to the z -axis. Thus, the mass-to-flux ratio of the region normalized by its critical value $(M/\Phi)_{\text{crit}} = (0.53/(3\pi))(5/G)^{1/2}$ is $\mu = 21$, 74, and 56, respectively. These values are much larger than the initial mass-to-flux ratio $\mu = 4$.

In figure 4, we show the evolution of the Ohmic, Hall, and ambipolar diffusion coefficients, η_O , η_H , and η_A , at the center of model Para as a function of the central density. The evolution of model Ortho and NoHall were almost the same. In $\rho_c < 10^{-14}$ g cm^{-3} , η_H is larger than η_A and η_O and the gas rotation is significantly affected by the Hall current term in this region. The value of η_H is much larger than the “critical value” for disk formation (thin black line) suggested by Krasnopolsky *et al.* (2011) in this region. Although the η_H decreases in $\rho_c \gtrsim 10^{-13}$ g cm^{-3} , the Ohmic and ambipolar diffusion alternatively play a role in $\rho_c \gtrsim 10^{-13}$ g cm^{-3} , and the rotation is maintained in the high density region without magnetic braking. Note that Krasnopolsky *et al.* (2011) only considered the Hall term and neglected other non-ideal effect. We remark that η_A does not strongly depend on $|\mathbf{B}|$ around $\rho \sim 10^{-14}$ g cm^{-3} although $\eta_A \propto |\mathbf{B}|^2$ in low density regions.

Because of the conservation of angular momentum, the spin-up due to the Hall term at the center causes spin-down of the outer region, eventually, causing anti-rotation against the disk. In figure 5, we show the cross section of the rotation velocity distribution of Model Para in the x - z plane at the same epoch of figure 1. This figure clearly shows an anti-rotating envelope surrounding the forward rotating inner region. Since the anti-rotation of envelope is driven by torsional Alfvén waves, the anti-rotating region expands with time and will propagate to the outside of the parental core. Thus,

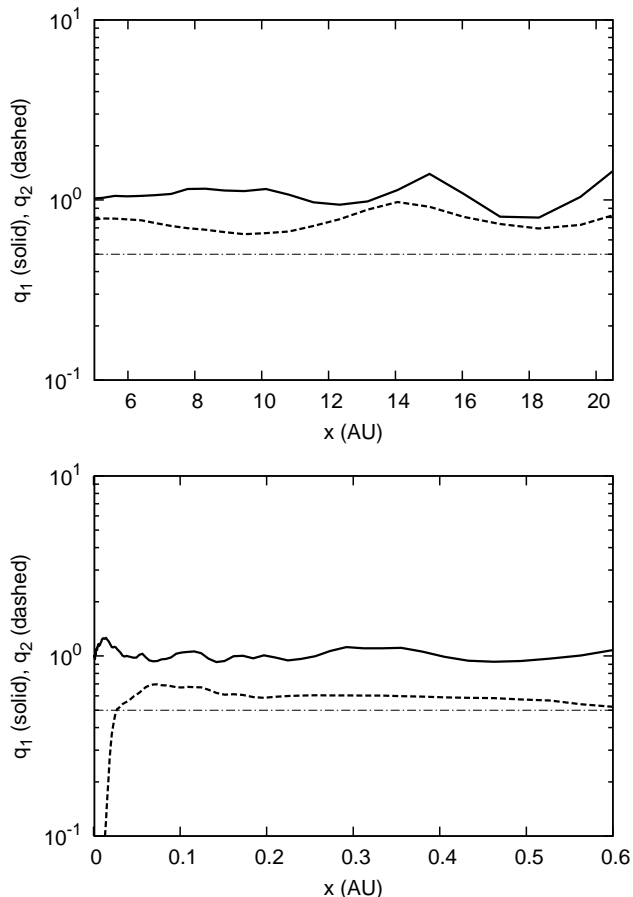


FIG. 2.— Solid lines show the ratio of the sum of the centrifugal force and the pressure gradient force to the radial gravitational force, $q_1 = \left| \frac{v_\phi^2/x + \nabla_r p/\rho}{\nabla_r \Phi} \right|$. Here, v_ϕ , p and Φ are the rotation velocity, gas pressure and the gravitational potential, respectively. The dashed lines show the ratio of the centrifugal force to the radial gravitational force, $q_2 = \left| \frac{v_\phi^2/x}{\nabla_r \Phi} \right|$. The dashed-dotted lines show $q = 0.5$. In the regions where the dashed lines are larger than the dashed-dotted lines, the gas is mainly supported by the centrifugal force. The top and bottom panels show the results of Models Para and Ortho, respectively. The epochs of each model are the same as those in figure 1.

the angular momentum of the direction opposite to the disk would eventually be cast away to the interstellar medium.

4. CONCLUSIONS AND DISCUSSION

In this study, we investigated the effect of the Hall current term on the formation of circumstellar disk. by considering all non-ideal effects as well as the radiative transfer are considered. To our knowledge, this is the first study that simultaneously includes these physical processes in a three-dimensional simulation.

We found that the disk evolution can be categorized into two cases depending whether the magnetic field and the rotation vector are parallel or anti-parallel. In the anti-parallel case, a relatively large ($r \gtrsim 10$ AU) and massive disk forms simultaneously with the protostar formation; however, a disk with $r \gtrsim 1$ AU does not form in parallel case. Thus, the parity of the magnetic field significantly changes the disk formation process which has not been paid much attention to so far. Since the parallel

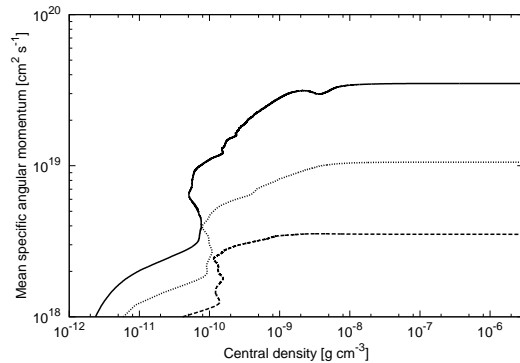


FIG. 3.— The time evolution of the mean specific angular momentum of the inner region with $\rho > 10^{-12}$ g cm $^{-3}$ as a function of the central density. The solid, dashed, and dotted lines show the results of Model Para, Ortho, and NoHall, respectively.

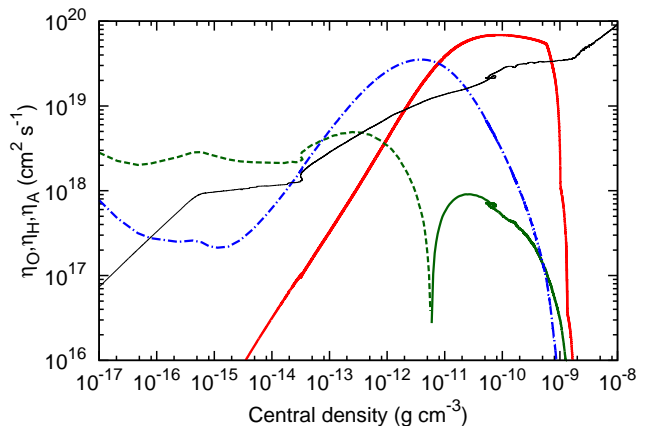


FIG. 4.— Magnetic diffusion coefficients, η_O , η_H , and η_A at the center as a function of the central density in Model Para. The red line shows η_O . The green line shows η_H where the dashed line shows the region of $\eta_H < 0$ and the solid line shows the region of $\eta_H > 0$, and the blue dashed-dotted line shows η_A . The black thin line shows the “critical value” of η_H , 3×10^{20} B $_c$ (cm 2 s $^{-1}$) suggested by Krasnopolsky *et al.* (2011) above which the disk is formed in their simulations. Here, B_c is the central magnetic field.

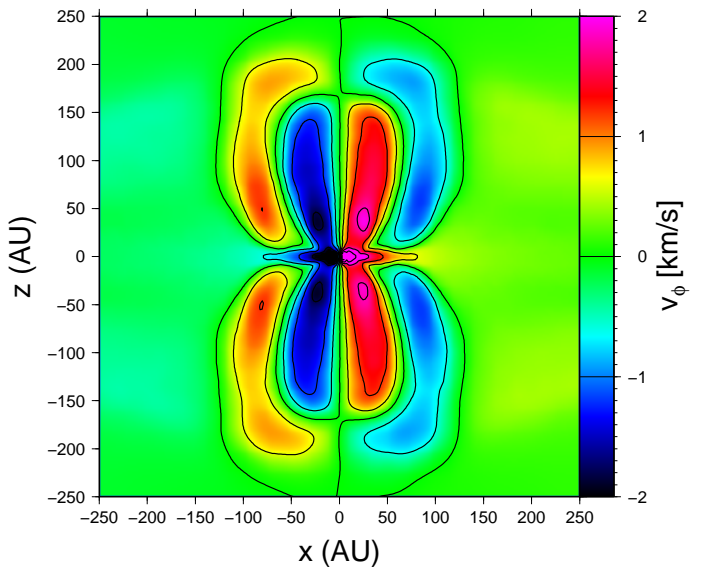


FIG. 5.— The cross section of v_ϕ in the x-z plane in Model Para. The epoch of the snapshot is the same as that in Fig. 1.

and anti-parallel properties are inherent and do not readily change in time, we expect that the spin-up (the magnetic braking weakening) and spin-down (the magnetic braking strengthening) effects due to the Hall current term are also important in the subsequent disk evolution and the difference between the two cases is maintained or enhanced. Therefore, we suggest that the disk evolution can be categorized into two cases. We may call the resultant parallel and anti-parallel systems as *Ortho-disk* and *Para-disk*, respectively.

Our results predict that the bimodality in the disk size distribution spontaneously arises due to the Hall current term in typically magnetized molecular clouds. We tend to think that the disk size has a unimodal distribution according to the strength of the rotation and the magnetic field of the cloud cores. However, as we have shown above, the Hall term changes the disk size according to the parallel or anti-parallel property of the cores. It is expected that about half of the molecular cloud cores have the parallel configuration and the others have the anti-parallel configuration because the Hall term would not play a role during the cloud core formation (Wardle 2004) and there is no physical mechanism which distinguishes the parallel and anti-parallel configurations. On the other hand, during the gravitational collapse of cloud core, the Hall term becomes effective and strengthens or weakens the magnetic braking. Therefore, the bimodality of the disk size distribution spontaneously arises from the unimodal distributions of the rotation and the magnetic field strength of the cores.

An observational signature predicted from our results is the anti-rotating envelope in the Class 0 YSOs. At the end of the simulations, the anti-rotating envelope had a size of $r \gtrsim 100$ AU and the rotation velocity of $v_\phi \sim 1$ km. Because the anti-rotation of the envelope stems from torsional Alfvén waves, the anti-rotating region expands with time. We predict future observations will find an anti-rotating envelope against disk rotation in the Class 0 YSOs. These observations will provide clear evidence that the Hall current term plays an important role for the evolution of circumstellar disks.

In this paper, several simplifications were adopted and their influences should be investigated in future works.

We employed a fixed dust grain size of $a = 0.035 \mu\text{m}$ and a fixed cosmic-ray ionization rate of $\xi_{\text{CR}} = 10^{-17} \text{s}^{-1}$ and the magnetic resistivities are sensitive to the models of dust and cosmic-ray (Dapp *et al.* 2012; Padovani *et al.* 2014). Furthermore, the drift velocity of the magnetic field induced by the Hall term which characterizes the strength of the Hall term, linearly depends on η_H . Thus, the simulations with the different models are necessary to confirm our results. The misalignment between the magnetic field and the rotation vector is another important issue. In our simulations, the initial rotation vector and the magnetic field are in perfectly parallel or anti-parallel configurations. However, it is expected that they are mutually misaligned in the realistic cloud cores (Hennebelle and Ciardi 2009; Joos *et al.* 2012). Its effect on the disk formation with non-ideal effects should also be investigated. We used a rigidly rotating shell as the outer boundary condition. Because of the angular momentum out-flux at the boundary, the total angular momentum is non-conserved quantity in our simulations. At the end of the simulations, the total angular momentum of Models Para, Ortho, and NoHall within the boundary shell was 97, 94.3, and 95.5 % of the initial angular momentum, respectively. Note that the difference of the angular momentum between models is expected because the Hall current term changes the angular momentum transfer rate near the boundary. Similar phenomena are also observed in the previous works. Previous simulations starting from the non-rotating core with the Hall term and outgoing boundary have a finite angular momentum at the end of the simulations (Krasnopolsky *et al.* 2011; Li *et al.* 2011). We expect the treatment of the outer boundary condition would not change our results significantly because the crossing time of Alfvén wave $t_{\text{cross}} = R/v_A$ is larger than the free-fall time t_{ff} (in our initial condition, $t_{\text{cross}}/t_{\text{ff}} = 2.5$) and the boundary mainly influences the relatively outer region within our simulation time $t_{\text{sim}} \lesssim 1.1t_{\text{ff}}$. However, more sophisticated boundary conditions are desired.

ACKNOWLEDGMENTS

We thank K. Tomida and Y. Hori for providing EOS table. The computations were performed on the XC30 system at CfCA of NAOJ.

REFERENCES

- T. C. Mouschovias and E. V. Paleologou, *ApJ* **230**, 204 (1979).
 R. R. Mellon and Z.-Y. Li, *ApJ* **681**, 1356 (2008),
 arXiv:0709.0445.
 P. Hennebelle and S. Fromang, *A&A* **477**, 9 (2008),
 arXiv:0709.2886.
 M. R. Bate, T. S. Tricco, and D. J. Price,
MNRAS **437**, 77 (2014), arXiv:1310.1092 [astro-ph.SR].
 N. Ohashi, K. Saigo, Y. Aso, Y. Aikawa, S. Koyamatsu, M. N.
 Machida, M. Saito, S. Z. Takahashi, S. Takakuwa, K. Tomida,
 K. Tomisaka, and H.-W. Yen, *ApJ* **796**, 131 (2014),
 arXiv:1410.0172.
 N. Sakai, T. Sakai, T. Hirota, Y. Watanabe, C. Ceccarelli,
 C. Kahane, S. Bottinelli, E. Caux, K. Demyk, C. Vastel,
 A. Coutens, V. Taquet, N. Ohashi, S. Takakuwa, H.-W. Yen,
 Y. Aikawa, and S. Yamamoto, *Nature* **507**, 78 (2014).
 J. J. Tobin, L. W. Looney, D. J. Wilner, W. Kwon, C. J.
 Chandler, T. L. Bourke, L. Loinard, H.-F. Chiang, S. Schnee,
 and X. Chen, *ArXiv e-prints* (2015),
 arXiv:1503.05189 [astro-ph.SR].
 R. R. Mellon and Z.-Y. Li, *ApJ* **698**, 922 (2009), arXiv:0809.3593.
 M. N. Machida, S.-i. Inutsuka, and T. Matsumoto,
MNRAS **438**, 2278 (2014), arXiv:1307.1747 [astro-ph.SR].
 K. Tomida, S. Okuzumi, and M. N. Machida,
ApJ **801**, 117 (2015), arXiv:1501.04102 [astro-ph.SR].
 Y. Tsukamoto, K. Iwasaki, S. Okuzumi, M. N. Machida, and S.-i.
 Inutsuka, *ArXiv e-prints* (2015a),
 arXiv:1503.04901 [astro-ph.SR].
 K. Tomida, K. Tomisaka, T. Matsumoto, Y. Hori, S. Okuzumi,
 M. N. Machida, and K. Saigo, *ApJ* **763**, 6 (2013),
 arXiv:1206.3567 [astro-ph.SR].
 M. Wardle and C. Ng, *MNRAS* **303**, 239 (1999),
 astro-ph/9810468.
 R. Krasnopolsky, Z.-Y. Li, and H. Shang, *ApJ* **733**, 54 (2011),
 arXiv:1101.3018 [astro-ph.SR].
 Z.-Y. Li, R. Krasnopolsky, and H. Shang, *ApJ* **738**, 180 (2011),
 arXiv:1106.2620 [astro-ph.GA].
 C. R. Braiding and M. Wardle, *MNRAS* **422**, 261 (2012),
 arXiv:1109.1370 [astro-ph.SR].
 M. N. Machida and T. Matsumoto, *MNRAS* **413**, 2767 (2011),
 arXiv:1008.0920 [astro-ph.SR].

- W. B. Dapp, S. Basu, and M. W. Kunz, *A&A* **541**, A35 (2012), arXiv:1112.3801 [astro-ph.SR].
- K. Iwasaki and S. Inutsuka, *MNRAS* **418**, 1668 (2011), arXiv:1106.3389 [astro-ph.GA].
- K. Iwasaki and S.-I. Inutsuka, in *Numerical Modeling of Space Plasma Flows (ASTRONUM2012)*, Astronomical Society of the Pacific Conference Series, Vol. 474, edited by N. V. Pogorelov, E. Audit, and G. P. Zank (2013) p. 239.
- S. C. Whitehouse and M. R. Bate, *MNRAS* **353**, 1078 (2004), arXiv:astro-ph/0406392.
- S. C. Whitehouse, M. R. Bate, and J. J. Monaghan, *MNRAS* **364**, 1367 (2005), arXiv:astro-ph/0509837.
- Y. Tsukamoto, K. Iwasaki, and S.-i. Inutsuka, *MNRAS* **434**, 2593 (2013a), arXiv:1305.4436 [astro-ph.SR].
- J. Wurster, D. Price, and B. Ayliffe, *MNRAS* **444**, 1104 (2014), arXiv:1408.1807 [astro-ph.SR].
- V. Alexiades, G. Amiez, and P.-A. Gremaud, *Com. Num. Meth. Eng* **12**, 12 (1996).
- M. N. Machida, S.-I. Inutsuka, and T. Matsumoto, *PASJ* **63**, 555 (2011a), arXiv:1009.2140 [astro-ph.SR].
- T. Sano and J. M. Stone, *ApJ* **570**, 314 (2002), astro-ph/0201179.
- D. Semenov, T. Henning, C. Helling, M. Ilgner, and E. Sedlmayr, *A&A* **410**, 611 (2003), arXiv:astro-ph/0308344.
- J. W. Ferguson, D. R. Alexander, F. Allard, T. Barman, J. G. Bodnarik, P. H. Hauschildt, A. Heffner-Wong, and A. Tamanai, *ApJ* **623**, 585 (2005), arXiv:astro-ph/0502045.
- S. Okuzumi, *ApJ* **698**, 1122 (2009), arXiv:0901.2886 [astro-ph.EP].
- T. C. Mouschovias and L. Spitzer, Jr., *ApJ* **210**, 326 (1976).
- T. Matsumoto and K. Tomisaka, *ApJ* **616**, 266 (2004), arXiv:astro-ph/0408086.
- M. N. Machida, S. Inutsuka, and T. Matsumoto, *ApJ* **670**, 1198 (2007), arXiv:astro-ph/0702183.
- C. Marois, B. Zuckerman, Q. M. Konopacky, B. Macintosh, and T. Barman, *Nature* **468**, 1080 (2010), arXiv:1011.4918 [astro-ph.EP].
- A. P. Boss, *Science* **276**, 1836 (1997).
- S. Inutsuka, M. N. Machida, and T. Matsumoto, *ApJ* **718**, L58 (2010), arXiv:0912.5439 [astro-ph.EP].
- M. N. Machida, S. Inutsuka, and T. Matsumoto, *ApJ* **729**, 42 (2011b), arXiv:1101.1997 [astro-ph.SR].
- Y. Tsukamoto and M. N. Machida, *MNRAS* **416**, 591 (2011).
- Y. Tsukamoto and M. N. Machida, *MNRAS* **428**, 1321 (2013), arXiv:1210.0526 [astro-ph.SR].
- Y. Tsukamoto, M. N. Machida, and S. Inutsuka, *MNRAS* **436**, 1667 (2013b).
- Y. Tsukamoto, S. Z. Takahashi, M. N. Machida, and S. Inutsuka, *MNRAS* **446**, 1175 (2015b), arXiv:1404.7271 [astro-ph.SR].
- M. Wardle, *Ap&SS* **292**, 317 (2004), astro-ph/0307086.
- M. Padovani, D. Galli, P. Hennebelle, B. Commerçon, and M. Joos, *A&A* **571**, A33 (2014), arXiv:1408.5901.
- P. Hennebelle and A. Ciardi, *A&A* **506**, L29 (2009), arXiv:0909.3190 [astro-ph.GA].
- M. Joos, P. Hennebelle, and A. Ciardi, *A&A* **543**, A128 (2012), arXiv:1203.1193 [astro-ph.SR].